Reassessment of 20th century global mean sea-level rise

Sönke Dangendorf[1], Marta Marcos[2], Guy Wöppelmann[3], Clinton Conrad[4], Thomas Frederikse[5], Riccardo Riva[5]

[1]University of Siegen, [2]University of the Balearic Islands, [3]LIENSs, Universite de La Rochelle-CNRS, [4]University of Oslo, [5]Delft University of Technology

Submitted to Proceedings of the National Academy of Sciences of the United States of America

The rate at which global mean sea level (GMSL) rose during the twentieth century is uncertain, with little consensus between various reconstructions that indicate rates of rise ranging from 1.3 to 2 mmyr^{-1}. Here we present a twentieth-century GMSL reconstruction computed using a novel area-weighting technique for averaging tide gauge records that (i) incorporates, for the first time, up to date observations of vertical land motion (VLM) and corrections for local geoid changes due to ice melting and terrestrial freshwater storage (TWS), and (ii) allows for the identification of possible differences compared to earlier attempts. Our reconstructed GMSL trend of 1.1±0.3 mmyr^{-1} (1σ) before 1990 falls below previous estimates, while our estimate of 3.1±1.4 mmyr^{-1} from 1993 to 2012 is consistent with independent estimates from satellite-altimetry, leading to overall acceleration larger than previously suggested. This feature is geographically dominated by the Indian-Ocean-Southern-Pacific region marking a transition from lower than average rates before 1990 towards unprecedented high rates in recent decades. We demonstrate that VLM corrections, area-weighting, and our use of a common reference datum for tide gauges may explain the lower rates compared to earlier GMSL estimates, in approximately equal proportion. The trends and multi-decadal variability of our new GMSL curve also compare well to the sum of individual contributions obtained from historical outputs of the Coupled Model Intercomparison Project Phase 5 (CMIP5). This, in turn, increases our confidence in process-based projections presented in the Fifth Assessment Report (AR5) of the Intergovernmental Panel on Climate Change (IPCC).

Global mean sea level | tide gauges | vertical land motion | fingerprints | climate change

Estimates of GMSL change before the advent of satellite altimetry (e.g. refs 1-6) rely on a historical data set of coastal tide gauges with an uneven spatial coverage biased towards the Northern Hemisphere and with limited temporal sampling (7) (**Fig. S1A and B**). These tide gauges are grounded on land and are thus affected by the vertical motion of the Earth's crust caused by both natural processes (e.g. glacial isostatic adjustment (GIA) following the last deglaciation or tectonic deformations) and anthropogenic activities (e.g. groundwater depletion and dam building). As pointwise measurements, tide gauges further track local sea levels which reflect the geographical patterns induced by ocean dynamics and geoid changes in response to mass load redistribution (8). Altogether, these factors hamper our ability to provide a unique twentieth-century GMSL reconstruction.

Consequently, several reconstructions of GMSL changes have been published over the past decade, each of them based on different data subsets, methodological approaches and tide gauge corrections. Among the most cited, ref. 1 and ref. 2 combined static spatial patterns constrained from satellite altimetry observations with temporal information from tide gauges into a global curve showing a twentieth-century GMSL rise of 1.7±0.3 mmyr^{-1}. Ref. 5 averaged regional sea level curves obtained from stacking rates of individual station data into a global reconstruction, leading to an increase of 1.9±0.3 mmyr^{-1} since 1900. These values, as well as others reported following similar approaches (3, 4), are consistent within their uncertainties and were subsequently adopted by the AR5 of the IPCC (9). More recently, ref. 6 developed a probabilistic approach that used tide gauges in combination with ensembles of model estimates for the spatial fingerprints of ocean dynamics, GIA and ice melting as well as an additional residual parameter for other local contributions to VLM (such as tectonics or geomorphology), resulting in a significantly lower rate of 1.3 mmyr^{-1}. A set of sensitivity experiments indicated that their methodological approach was the primary reason for their estimate of a slower GMSL rate. Ref. 6 therefore suggested that previous studies have overestimated twentieth-century GMSL rise and thus provided one possible solution of the enigma formulated more than a decade ago by Walter Munk (10).

This enigma points out that previous estimates of twentieth-century GMSL rise (e.g. refs.1-5) are too linear and larger than estimates of the sum of individual contributions (thermal expansion, ice melt and terrestrial water storage) (9). Although some attempts have been made to explain these discrepancies on the basis of underestimated sources (e.g. ref. 11), ref. 6 highlighted that their lower rate naturally balances the global sea level budget as the sum of modelled thermal expansion, glacier melting and land water storage from the tabulations in the AR5 (9) without requiring any additional contribution from the ice sheets in Greenland and Antarctica. Ref. 12 recently extended this modelled GMSL budget with estimates of the contribution of the ice-sheets using CMIP5 historical runs as forcing. However, as discussed in ref. 13, the GMSL reconstructions, especially those that show a larger twentieth-century trend, still exhibit remarkable differences to the CMIP5-based GMSL estimates. Particularly striking is a significant mismatch of observed and modelled GMSL between the

Significance

Estimates of GMSL before the advent of satellite-altimetry vary widely, mainly due to the uneven coverage and limited temporal sampling of tide gauge records, which track local sea level rather than the global mean. Here we introduce a novel approach that combines recent advances in solid Earth and geoid corrections for individual tide gauges with improved knowledge about their geographical representation of ocean internal variability. Our new assessment (i) yields smaller trends before 1990 than previously reported leading to a larger overall acceleration, (ii) identifies three major explanations for differences with previous estimates, and (iii) reconciles observational GMSL estimates with the sum of individually modelled contributions from the Coupled Model Intercomparison Project 5 database over the entire twentieth century.

Reserved for Publication Footnotes

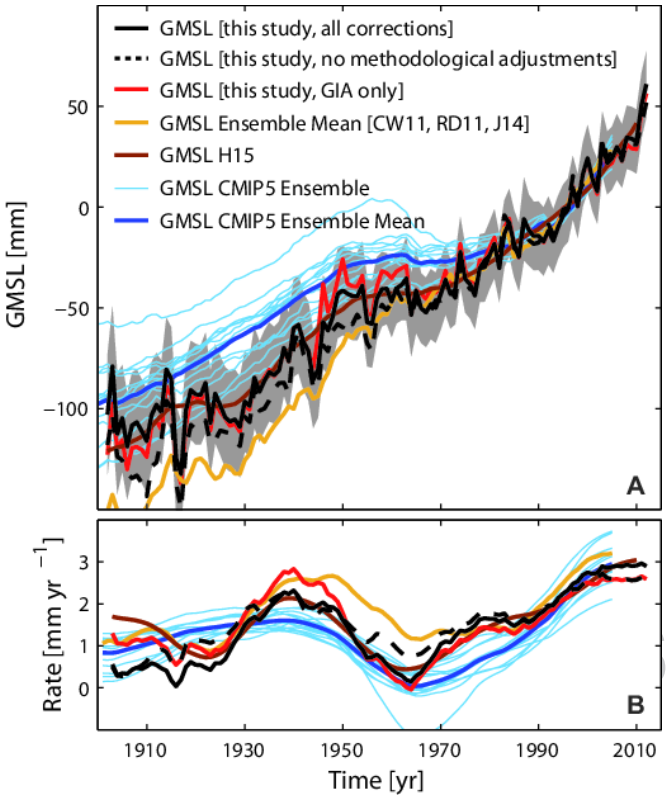

Fig. 1. | Time series and rates of GMSL over the period 1902-2012. A Revised GMSL reconstruction based on 316 tide gauges in comparison to previous estimates and modelling attempts based on historical CMIP5 models (12). The grey shading marks the 1σ errors of the final reconstruction. The dotted black line represents a GMSL reconstruction with all VLM and geoid corrections, but without methodological adjustments such as area weighting and the use of a common mean. **B** The corresponding rates calculated with a SSA using an embedding dimension of 15 years.

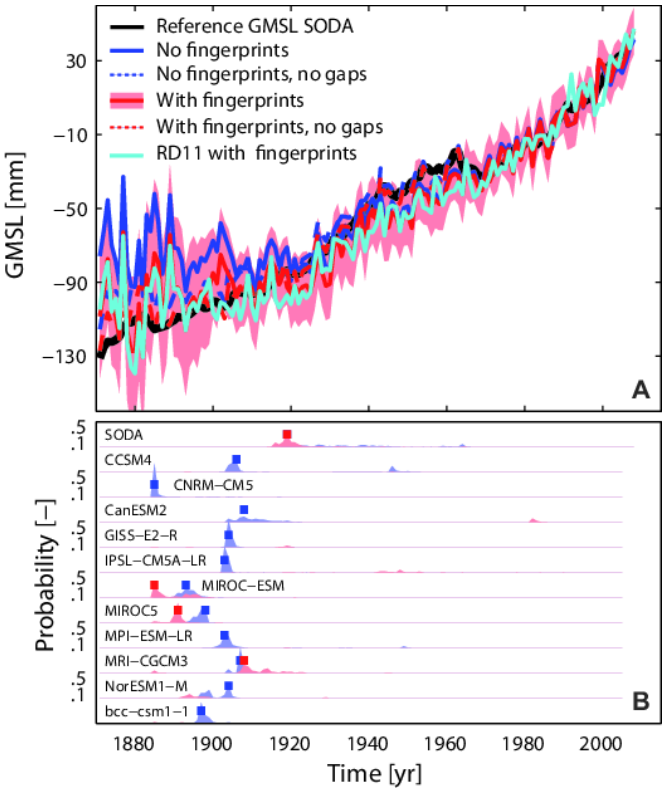

Fig. 2. | Performance of the area-weighted average approach in ocean models. A Sensitivity of the area weighted average technique in the SODA reanalysis (its reference GMSL is shown by the black line) to the four initial data sets: (1) Gaps as in reality, no fingerprint corrections applied (dark blue), (2) assuming a full record, no fingerprint corrections applied (dark blue dotted), (3) gaps as in reality, fingerprint corrections applied (red, with shading noting its 1σ uncertainty), and (4) assuming a full record, fingerprint corrections applied (red dotted) (see **Fig. S3** for the respective curves from the 11 CMIP5 based synthetic sea level fields). The cyan curve represents a GMSL reconstruction with gaps as in reality and fingerprint corrections applied, but using the tide gauge subset from ref. 2. **B** Results of the Bayesian change point analysis (25) on the differences between each model specific reference GMSL and corresponding tide gauge reconstruction (blue = without fingerprint corrections; red = with fingerprint correction) in each model. The change point analysis provides statistically the probability and timing of changes (shaded areas) in the relationship between the "true" model GMSL and its reconstruction. Tall thin spikes suggest relative certainty in the timing of a change point, while wider spikes suggest more uncertainty in its timing. The red and blue squares mark the most probable timing from 500 iterations.

1930s and the 1970s, where the models generally suggest lower rates than observations. Up to now it is unclear whether this mismatch stems from poor model performances or uncertainties in individual GMSL reconstructions (both in variability and long-term trends) (13).

Although ref. 6 used probabilistic sea level fields to show why previous GMSL reconstruction approaches overestimated the rise before 1990, their tests have two general limitations: First, their values only account for a fraction of the GMSL overestimates during this period, and second, their sensitivity experiments rely on their reconstructed sea level field rather than original tide gauges. Ref. 14 additionally suggested that the specific tide gauge selection of the ref. 6 study could have biased the 20th century GMSL towards lower rates. Specifically, they pointed towards the high uncertainties of Artic tide gauges, which were excluded in previous studies either because of the lack of altimetry data in the region or as a result of their questionable quality. In a very recent study, ref. 15 further investigated in Monte-Carlo-experiments the probability that 15 of the longest tide gauges (showing an average rate of 1.6 mmyr^{-1}) can be biased high or low relative to the global mean due to the contributions of ocean dynamics, GIA and present day ice melt. Assuming independence between the different sources, they suggested a probability of less than 1% that the rates obtained from these 15 tide gauge records are consistent with global mean rates lower than 1.4 mmyr^{-1}. These contrary arguments suggest that the spread between individual reconstructions is still poorly understood. Furthermore, none of the available reconstructions utilize local constraints on VLM, and they do not incorporate TWS changes.

Here we present a new GMSL reconstruction since 1902 that, for the first time, accounts for ocean volume redistribution, local observations (mostly GPS) of VLM and geoid changes due to ongoing GIA, present-day ice-melt and TWS including groundwater depletion and water impoundment behind dams. We base our approach on a novel area-weighting average technique and on recent scientific achievements made for each individual correction. Our tide gauge selection is based on the data set described in ref. 16 consisting of 322 stations (**Fig. S1A**), for which VLM corrections with uncertainties of less than 0.7 mmyr^{-1} are available (see *Materials and Methods* and **Fig. S2A**). After accounting for VLM, each tide gauge is further corrected for geoid changes from ongoing GIA (17), glacier/ice-sheet melting (18-20) (**Fig. S2C and D**) and TWS (21, 22) (**Fig. S2B**). The tide gauges are then grouped into six coherent regions objectively defined to account for water volume redistribution (**Fig. S1A**) (20). Ref.

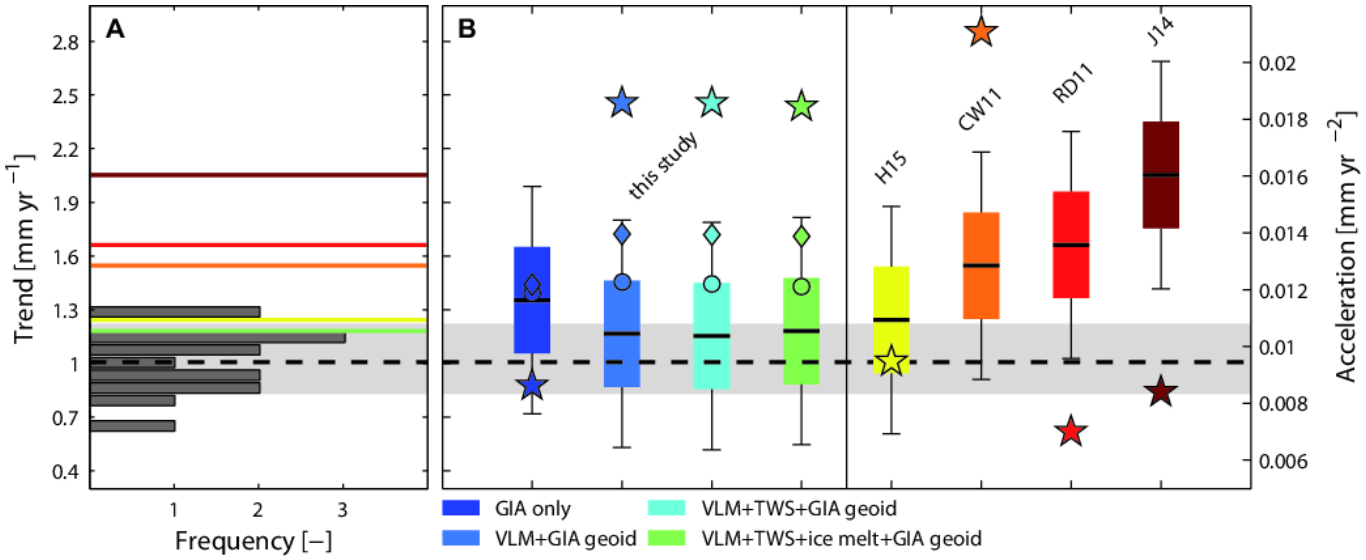

Fig. 3. | Linear trends in observed and modelled GMSL over the period 1902-1990. A Linear trend frequency in the CMIP5 GMSL ensemble from ref. 12 (dark grey bars) together with the median value (thick dotted line) and the 68% confidence bounds (light grey shading). The color coding follows **B**. **B** Linear trends of four different GMSL realizations based on different corrections applied in comparison to previous estimates with their respective uncertainties (based on ref. 25) as boxplots (1σ and 2σ uncertainties). The dots correspond to the trends when no area weighting is applied, while the diamonds provide trend estimates for the reconstructions based on rate stacking without area-weighting as in ref. 5. Also shown is the acceleration term (pentagrams, right y-axis) for each reconstruction extracted from the first differences of the non-linear trends over the entirely available period of each reconstruction since 1902.

23 demonstrated that these regions co-vary to some extent, so that an average between them cancels out some of the regional variability leading to an improved estimate of the "true" GMSL. Within each oceanic region, a regional mean sea level curve is built by recursively combining the two nearest stations into a new virtual station halfway until only one station is left. The procedure is similar to the so-called virtual station technique developed by ref. 5, but with two important differences: first, to account for an unknown reference datum, we stack records adjusted for a common mean (i.e. removing in each record the mean of a common period of at least 19 years) rather than averaging their rates. Second, our GMSL reconstruction accounts for the spatial area of each of the six oceanic regions for which the virtual stations are representative. We use this straightforward approach because of its reproducibility, the ability to perform numerous sensitivity studies with limited computational effort, and the fact that ref. 23 obtained comparable results for the multi-decadal variability in GMSL as more complex approaches based on empirical orthogonal functions (1).

Our resulting GMSL reconstruction (using the subset for which the VLM uncertainty is smaller than 0.7 mmyr^{-1}) is displayed in **Fig. 1A**, indicating a long-term trend of 1.3±0.2 mmyr^{-1} (P>0.99) since 1902 (here we report the error considering long-term persistent variability as modelled in ref. 24). This value is consistent with ref. 6 but lower than those considered by the IPCC AR5 (9) represented here by the ensemble average of observed GMSL curves from refs. 1, 2 and 5 (rates of individual reconstruction can also be found in the **Fig. S8**). Over the period 1993 to 2012 our reconstruction yields a trend of 3.1±1.4 mmyr^{-1} (P>=0.97) similar to the values obtained from independent satellite altimetry measurements (e.g. ref. 9). When comparing rates (**Fig. 1B**) there is a close correspondence of all tide gauge reconstructions after 1970, while before that time some remarkable differences appear. For instance, our new GMSL curve shows, as ref. 6, rates close to zero at the beginning of the 1960s, whereby the manifestation of this drop is stronger than in earlier assessments (1, 2, 5), which yield minimum rates of only roughly 1 mmyr^{-1}. Before the 1960s the reconstructions from ref. 1, 2, and 5 also suggest consistently larger rates than our new GMSL curve, which is mainly related to our application of VLM and geoid corrections, rather than GIA only (**Fig. 1B**). These corrections play an increasingly important role in the earlier decades where the geographical bias of sparse tide gauge records is particular strong (**Fig. S1B**) and might also explain the lower rates before ~1920 compared to ref. 6, who treated the VLM problem by using probabilistic model ensembles instead of local VLM observations as used here. This also means that during this period the robustness of our GMSL curve depends on the quality of the VLM and geoid corrections at a very few locations.

To explore whether the lower rates in our new GMSL reconstruction (**Fig. 1B**) before ~1970 are the result of methodological limitations with respect to the heterogeneous spatial and temporal tide gauge distribution, we test our approach in a set of 12 synthetic sea level fields from the SODA reanalysis and historical simulations of CMIP5 models over their common period from 1871-2005; these are combined with the corresponding components of the glacier contribution (in case of SODA: the glacier reconstruction from ref. 18), and historical fingerprints from TWS (21, 22) and the Antarctic and Greenland ice sheets (19, 20) (see *Materials and Methods*). Since in the synthetic sea level fields the true model GMSL, as well as the individual ice-melt and TWS fingerprints, are a priori known, they are an excellent testbed for our reconstruction approach. From each synthetic sea level field we therefore assembled four different surrogate data sets, which are sampled at the 322 tide gauge locations used in reality (see *Materials and Methods*): with and without realistic data gaps and with and without corrections for the regional deviations from the global mean due to ice-melt and TWS fingerprints. The comparison of the reconstructed GMSL curves with the true reference GMSL of each model (**Fig. 2A** for the SODA model and **Fig. S3** for the 11 CMIP5 models) confirms that it is indeed the availability of tide gauge records that primarily hampers robust GMSL estimates leading to large biases mainly in the earlier decades around the turn-of-the-century. To objectively identify the timing of these biases we apply a Bayesian change point analysis (25) to the residuals between the reference GMSL and each tide gauge reconstruction. This analysis identifies the posterior probability of a statistically significant change in the

residuals (P>=.95), i.e. the timing at which our approach is no longer able to reconstruct the true model GMSL. We identify significant change points between 1885 and 1919 for all models without the consideration of local fingerprint corrections, but these change points disappear in eight models after correcting individual tide gauge surrogates for their respective TWS and ice-melt fingerprint (**Fig. 2B**). From the remaining four models only two, SODA and MRI-CGCM3, suggest significant change points after 1902 (1919 and 1908, respectively), whereby their influence on the long-term trends since 1902 is only minor in the respective models (0.04 and 0.03 mmyr^{-1}, respectively (**Fig. S4B**). In general, the application of spatially varying corrections associated with ice-melt and TWS fingerprints reduces the trend biases in models from -0.45±1.17 mmyr^{-1} (median ± stdv. of the entire ensemble) to -0.02±0.70 mmyr^{-1} prior to 1902 (**Fig. S4A**). Although some uncertainties in the GMSL reconstructions still persist, most models indicate a reasonable performance (trend differences of 0.10±0.07 mmyr^{-1}with fingerprint corrections compared to 0.14±0.14 mmyr^{-1}without fingerprint corrections) of our approach with respect to long-term changes over the entire 20th century (**Fig. S4B**).

We also tested whether our approach is able to reconstruct the inter-annual to multi-decadal GMSL variability in the synthetic model fields (**Fig. S4C**). We find that our approach sufficiently reproduces the variability patterns in most models if all fingerprint corrections are applied (r = 0.78 ± 0.17 and r = 0.63 ± 0.21 with and without fingerprint corrections, respectively), whereby again a strong coupling to the availability of tide gauge records is recognized (r = 0.91 ± 0.11 assuming full tide gauge records without any gaps) (**Fig. S4C**). In SODA (the only model that assimilates temperature and salinity observations) a large drop following the volcanic eruption of Mount Agung from 1963 (e.g. ref. 11) is not well reproduced because of incomplete tide gauge records (**Fig. 2A**), leading to a poorer representation of the inter-annual variability (r = 0.45) compared to the CMIP5-based models (r = 0.79 ± 0.15) (**Fig. S4C**). However, reconstructions of GMSL from other CMIP5 models showing comparably large drops at the same time (e.g. GISS-E2-R, MIROC-ESM) perform well in reproducing such variations (r = 0.95 and r = 0.79, respectively) (**Fig. S3, Fig. S4C**). Furthermore, in reality our new GMSL curve shows, together with that of ref. 6, the most pronounced drop of all reconstructions (**Fig. 1B**). This (together with the lower rates before) leads also to a better agreement to the historical CMIP5 simulations of the GMSL budget compiled by ref. 12, which indicate generally more moderate rates between the 1930s and 1970s than the tide gauge reconstructions from ref. 1, 2 and 5 (**Fig. 1B**).

To further examine the influence of methodological adjustments as well as VLM and geoid corrections on pre-altimetry GMSL rates, we produced a set of observation-based reconstructions with and without individual adjustments and corrections and calculated linear trends over the period 1902-1990 (**Fig. 3B**). First, we consecutively introduced the VLM and the individual geoid corrections for TWS and ice-melt in each tide gauge record. The corrections significantly reduce the spatial variability in each subregion with a particularly striking reduction in the Northeast Pacific (**Fig. S5**). Especially the tide gauges along the coast of Alaska are strongly affected by the corrections. In most cases the corrections lead to a reduction in the overall rate for the entire region and therefore also in the resulting GMSL, accounting for ∼0.2-0.3 mmyr^{-1} of the obtained differences compared to earlier estimates, whereby VLM itself plays the most important role (**Fig. 3B**). This contrasts with recent results by ref. 26 finding a VLM influence on GMSL of opposite sign but considering only large-scale VLM effects rather than local movements at the individual tide gauges. Second, we test the influence of using a common mean rather than stacking first differences, which was the preferred approach in most previous studies (e.g. refs. 1, 4 and 5) for solving the problem of an uncommon reference datum between individual tide gauges (colored diamonds in **Fig. 3B**). Using a common mean also results in ∼0.2-0.3 mmyr^{-1} lower trends than stacking rates. This is due to drifts resulting from an error accumulation in the integration process of the virtual stations that is especially relevant for the lower frequencies (2) (**Fig. S5**) and leads to artificially large rates in GMSL before ∼1960 (see sensitivity experiment in the SODA fields in **Fig. S6**). Comparing the corresponding six regional curves with the individual tide gauge records in each oceanic region suggests everywhere larger correlations when a common mean adjustment is used (**Fig. S5**). Third, we reconstructed the GMSL with and without area-weighting (colored dots in **Fig. 3B**). Regional averaging to reconstruct GMSL with and without area-weighting leads to differences of 0.2-0.3 mmyr^{-1}, due to the larger influence of comparably small areas (lowest trends before 1990 have been found in the Indian Ocean and South Pacific region, the South Atlantic, and the Northwest Pacific (**Fig. S7**)). The combination of all adjustments and corrections sums to ∼0.6-0.9 mmyr^{-1}, which potentially explains all of the differences compared to earlier assessments (ref. 1-5) of the 1902-1990 period. For the same period the sum of modeled contributions from the 14 member CMIP5 model ensemble by ref. 12 (see *Supplementary Text*) shows a median trend of 1 mmyr^{-1} (1σ bounds of 0.83-1.22 mmyr^{-1}) (**Fig. 3A**), which is consistent with our final GMSL estimate of 1.1±0.3 mmyr^{--1} (P>0.99) containing all necessary corrections (**Fig. 3A and B**). However, with the exception of ref. 6 all other published reconstructions clearly fall outside the range of modeled contributions (**Fig. 3A**).

The downward correction of previous pre-satellite altimetry GMSL estimates in combination with the close correspondence between satellite altimetry, historical CMIP5 simulations and our GMSL reconstruction after 1993 (**Fig. 1B**) has another important consequence: the trend difference between both periods leads to an acceleration (here estimated with a linear fit to the first differences of the non-linear trend obtained with a Singular Spectrum Analysis (SSA) using a smoothing window equal to 15 years and uncertainties obtained with a bootstrapping approach producing 100 surrogates) of 0.018±0.008 mmyr^{-2} (P>0.99) in GMSL, which is almost twice as large as in all other reconstructions (including ref. 6) except for the ref. 1 estimate (**Fig. 3B**). However, the rates of the GMSL reconstruction by ref. 1 are, with values exceeding 4 mmyr^{-1}, biased high compared to satellite altimetry since 1993 (**Fig. S8A**). To test the influence of this overestimation during the satellite altimetry period, we have substituted the satellite-based GMSL reconstruction from AVISO into ours and the reconstruction of ref. 1 for the period 1993-2012 (**Fig. S8A**). While our estimate is only barely affected by the adjustment (rates and acceleration become slightly higher), the acceleration in the ref. 1 reconstruction decreases considerably leading to a smaller value than in our reconstruction (**Fig. S8B**). This shows that the larger acceleration in the ref. 1 reconstruction should be considered with care. The acceleration in our GMSL curve is mainly determined by a transition from slower than average rates before 1990 (**Fig. S7A**) towards unprecedented high rates during the last two decades in the Indian Ocean South Pacific sector (**Fig. S7B**), which is consistent with an asymmetry in ocean mass redistribution between the Northern and Southern Hemisphere as suggested in ref. 23. The acceleration in GMSL is further consistent with recent findings that the anthropogenic contribution to GMSL (dominated by glacier melting and thermosteric sea level rise) has increased over the twentieth-century from less than 16% before 1950 to more than 69% after 1970 (12, 27, 28).

We have reassessed twentieth-century GMSL estimates from tide gauges by combining, for the first time, recent advances in

solid Earth and geoid corrections related to VLM, TWS and glacier/ice-sheet melting with an improved technique cancelling out ocean mass redistribution between individual regions (23). Our technique is simple, computationally efficient and allows us to evaluate the influence of each applied correction on GMSL estimates. The resulting GMSL curve shows, in agreement to ref. 6, significantly smaller trends compared to former and widely accepted GMSL estimates (9).This smaller rate is geographically dominated by slower than average sea level rise in the less well-instrumented Southern Hemisphere (29) and the Northwest Pacific compared to slightly larger than average rates in the North Atlantic (Fig. S7). The resulting trend gradient between the different regions is broadly consistent with the possible sea level imprint of a twentieth-century slowdown of the Atlantic Meridional Overturning Circulation (30) known from ocean model experiments (31), which, however, requires further investigations in future studies. Sensitivity experiments on the reasons for our lower pre-Altimetry GMSL rate compared to earlier attempts suggest that roughly one third of the obtained differences are related to biases stemming from regional variability due to VLM, TWS and ice-melt, while two thirds can be considered as methodological, i.e. resulting from an improved consideration of the geometry of regional sea level (here simple area-weighting) and a solution for overcoming the varying reference datum in individual tide gauge records (here a common mean). In contrast to ref. 15, who considered GMSL rates below 1.4 mmyr^{-1} being extremely unlikely, we used observational estimates of VLM and the spatial bias at tide gauges due to sea level fingerprints, thus avoiding any assumption about dependencies between different sea level contributions. Since our approach is different than that of ref. 6, our results provide an independent confirmation of their suggestion of a relatively slow pre-altimetry rate of GMSL rise. Our constraint of 1.1±0.3 mmyr^{--1} ($P>0.99$) during this period, in turn, explains the majority of the observed differences between individual reconstructions and recently modelled contributions to GMSL rise from the CMIP5 ensemble between the 1930s and 1970s, thus increasing our confidence in process-based models that are an indispensable tool for future projections (9).

Materials and Methods

Area-weighted average technique. Tide gauges only poorly sample the global ocean and their distribution has a large bias towards the Northern Hemisphere especially in the earlier decades of the twentieth-century (**Fig. S1**). To overcome this bias ref. 5 introduced a virtual station technique, in which the global ocean is divided into 12 coastal regions. For each coastal region, the two closest stations are recursively identified and stacked to a new virtual station weighted by their distance (for details on the error calculation see ref. 32). The 12 finally resulting virtual stations are then later further merged into a global curve. However, the final merging does not contain any further area-weighting, since the representativeness of the virtual station for a certain open ocean region is not known. Here we adopt the general idea of the approach, but improve it in several ways. First, we use different oceanic regions, which are based on an objective cluster analysis by ref. 23. The authors identified six coherently varying oceanic regions (**Fig. S1A**) from satellite altimetry and showed that a certain number of tide gauges are able to describe the multi-decadal variations within each region. The selection of these regions allows us to better sample the entire ocean and, more importantly, provides an estimate of the area for which each virtual station is representative. Hence, each virtual station can later be weighted before being merged into a global mean. The second adjustment is related to the reference problem of individual tide gauges. Since there is no common reference datum for the tide gauge records, ref. 5 stacked rates of mean sea level. However, one drawback of this approach is that small errors in individual estimates can inflate as the series is integrated backwards, with the lowest frequencies being most susceptible to errors (2). As a result the final global curve may drift away from the "truth" especially in the earlier years, where the uncertainties are significantly higher than in recent decades. To overcome this problem we stack two stations into a new virtual station by simply adjusting both records to a common mean. This, of course, presumes that two records always share a common period, which is the case in our tide gauge selection. The error propagation from an individual tide gauge towards the global mean is calculated following the approach of ref. 5 and ref. 32, which utilizes the geographical location of individual tide gauges.

Tide gauge records and corrections. We use an initial data set of 448 tide gauge records from the Permanent Service of Mean Sea Level (PSMSL) (7) for which VLM corrections from either GPS or tide gauge minus altimetry were available (15). The records are corrected for the mean seasonal cycle by fitting an annual and semi-annual harmonic to the monthly raw data. Also removed is the inverse barometer effect due to the hydrostatic response of the ocean to sea level pressure fluctuations around the spatial mean of the sea level pressure over the ocean (33) using the Twentieth-Century Reanalysis Project version two data set (20CRv2) (34).

VLM at tide gauges is adopted from ref. 16 (**Fig. S2A**). Stations for which a continuous GPS station is available are adjusted using the rates and uncertainties provided by ULR6a (note that this is an update of ref. 16 who used ULR5). If GPS is not available at a particular station, VLM is alternatively determined by differencing altimetry and tide gauge time series for their common period. Uncertainties are computed considering the noise content in the differenced time series as a combination of white noise and power law noise of an a priori unknown spectral index (16). The accuracy of the VLM correction is used to derive eleven different subsets of tide gauges, namely only those for which VLM is known with an uncertainty smaller than 0.5 mmyr^{-1} (228 stations), 0.6 mmyr^{-1} (283 stations),..., or 1.5 mmyr^{-1} (448 stations). The subset with an uncertainty smaller than 0.7 mmyr^{-1} (322 stations) is used for our final GMSL curve, which represents a trade-off between good data coverage and robust VLM estimates. Note that the differences between the GMSL curves from different tide gauge subsets based on VLM errors were found to be small (**Fig. S9**). Selection criteria based on earlier assessments (2) (e.g. only the longest tide gauges with high confidence on their quality) also showed only minor differences compared to our subsets in the SODA test fields (**Fig. 2A**) as well as observational data (1.3 mmyr^{-1} compared to our final estimate of 1.1 mmyr^{-1} before 1990) with VLM corrections applied only to those tide gauges that are covered in both subsets. For the comparison to earlier assessments also a GIA only correction is applied. In this case the ICE5G model by ref. 17 is used.

Changes in TWS (either caused by groundwater depletion or water impoundment behind dams) are accompanied by regional deflections of the solid earth (crustal motion) and sea surfaces (geoid), which can be calculated using Green's functions for vertical displacement and gravitational potential (21, 22). For water impoundment behind dams we use updated fields calculated by ref. 22 from 1902 to 2014, which are based on a combination of the global reservoir data sets from ref. 35 and ref. 36 (see ref. 22 for further details) consisting of 674 of the largest reservoirs. For groundwater depletion we adopt the fields from ref. 21 updated for the entire period from 1902 to 2014 and scaled to match recent estimates (37). Specifically, we used spatial variations from the hydrological model of ref. 36, which expresses groundwater depletion in a yearly resolution on a 0.5°*0.5° grid, and the scaled depletion rates everywhere by a factor of 0.8 so that total GWD matches the results of updated hydrological models (37). Since the crustal motion component is already approximated by the VLM correction, we only correct for spatial variations in the geoid response due to loading by changes in TWS (that is, deflections about a zero mean).

The same applies to the regional fingerprints from ice melting. To account for the regional deflections following freshwater injections from glaciers and ice sheets into the ocean we calculated fingerprints for updated sea level equivalents of 18 major glacier regions and ice sheet mass balance discharge estimates of the Greenland and Antarctic ice sheets. The glacier fingerprints are based on reconstructions from ref. 18 and their update in ref. 39. The Greenland ice sheet contribution to sea level is estimated using the recent mass balance estimate from ref. 19. The Antarctic ice sheet is modelled with the RACMO2.3 model (40) as in ref. 20, assuming (i) no mass changes before 1979, (ii) long-term balance between the surface mass balance from RACMO2.3 and ice discharge between 1979 and 1993, and (iii) small acceleration in ice discharge after 1993 to match GRACE estimates (20). The fingerprints for the ice melt contributions are calculated by solving the elastic sea level equation as described by ref. 41. The rotational feedback is included following ref. 42. As for TWS, we only considered the geoid response to the loading, which determines the regional deviations from the global mean.

Synthetic sea level data. One general problem of all tide gauge based GMSL reconstructions is that there is no observational validation option over more than two decades (satellite altimetry) available. An alternative possibility to test our approach is the use of artificial ocean model fields, where the "true" model GMSL is a priori known. However, so far there are no CMIP5 models available integrating simulations of the ocean and the cryosphere into coupled runs, so that except for the dynamic sea surface height each individual component has to be calculated offline. To produce homogeneous synthetic fields of historical sea level fields we combine historical fields of sea surface height from CMIP5 models and the SODA reanalysis over the period from 1871 to 2005 with independent estimates of glacier melting (18). Additionally added are the observation-based estimates of the ice sheets (19, 20) and TWS containing both groundwater depletion (21) as well as water impoundment behind dams (22). For the simulation of ocean dynamics sea surface height fields (variable 'zos' in CMIP5 terminology) are obtained from the historical simulations of 11 CMIP5 models (see **Fig. S3** for the models). For each model run, the globally averaged steric sea level (variable 'zosga'), corrected (quadratic fit to the control runs) for drifts due to the short spin-up

and integration time of the historical runs (11), is added to the sea surface height to account for global ocean volume changes within the model (43). CMIP5 runs were not further corrected for omitted pre-industrial volcanic forcing or additional drifts (see also ref. 12), since these corrections are globally uniform and will therefore not affect our model internal tests of the GMSL reconstruction technique. The SODA reanalysis (44) is also used and processed in the same way. Sea level changes associated with glacier melting (i.e. their total GMSL contribution including the respective regional fingerprint) are added to the modeled sea surface heights by multiplying the CMIP5 model specific glacier reconstruction from ref. 18 and ref. 39 with the respective fingerprint from ref. 45. For the SODA model the observational glacier reconstruction based on HADCRU forcing is used (18). All model fields are supplemented with the same observational fields of the ice-sheet and TWS contribution to sea level. For each modeled sea level field a GMSL was reconstructed based the area-weighted average technique applied to the grid point time series next to the real-world locations of tide gauges and then compared to the "true" reference GMSL of each model.

Trend uncertainties in individual GMSL reconstructions. The calculation of linear trends is susceptible to series of high/low values at the end of the time series. The corresponding uncertainty is usually addressed by simulating the natural variability, represented by the residuals around the trend line, in Monte-Carlo experiments under the assumption that it follows a specific noise process (e.g. ref. 46). While it has been widely accepted that an autoregressive process of the order 1 (AR1) is suitable for this purpose (e.g. ref. 9), recent studies demonstrate that the use of long-memory processes provides a physically more consistent description of the noise (24, 28, 47, 48, 49, 50). Ref. 24 further pointed out that none of the available GMSL reconstructions provides a proper description of the natural GMSL variability, since they are "trained" to reproduce the long-term trends (4). The authors therefore provided an improved estimate on the basis of ocean reanalysis data, which is used here uniformly for each GMSL reconstruction.

1. Church JA, White NJ (2011) Sea-level rise from the late 19th to the early 21st Century. *Surveys in Geophysics*, 32, 585-602.
2. Ray RD, Douglas BC 2011 Experiments in reconstructing twentieth-century sea levels. *Prog. Oceanogr*., 91, 496–515.
3. Wenzel M, Schroeter J. (2010) Reconstruction of regional mean sea level anomalies from tide gauges using neural networks. *J. Geophys. Res*., 115, C08013.
4. Calafat FM, Chambers DP, Tsimplis MN (2014) On the ability of global sea level reconstructions to determine trends and variability. *J. Geophys. Res.*, 119, 1572–1592.
5. Jevrejeva S, Moore JC, Grinsted A, Matthews AP, Spada G (2014) Trends and acceleration in global and regional sea levels since 1807. *Global and Planetary Change*, 113, 11-22.
6. Hay CH, Morrow E, Kopp RE, Mitrovica JX (2015) Probabilistic reanalysis of twentieth-century sea level rise. *Nature*, 517, 481–484.
7. Holgate SJ, et al (2013) New data systems and products at the Permanent Service for Mean Sea Level. *J. Coast. Res*., 29, 493–504.
8. Kopp RE, Hay CC, Little CM, Mitrovica JX (2015) Geographic variability of sea-level change. *Curr Clim Change Rep*, DOI 10.1007/s40641-015-0015-5.
9. Church, JA et al. (2013) Sea Level Change. *Climate Change 2013: The Physical Science Basis. Contribution of Working Group I to the Fifth Assessment Report of the Intergovernmental Panel on Climate Change*, eds Stocker, TF, et al., Ch. 13, Cambridge Univ. Press.
10. Munk W (2002) Twentieth century sea level: An enigma. *Proc. Natl. Acad. Sci. USA*, 99, 6550–6555.
11. Gregory J., *et al*. (2013) Global mean-sea level rise: is the whole greater than the sum of all prats? *J. Climate*, 26:13, 4476-4499.
12. Slangen ABA, *et al.* (2016) Anthropogenic forcing dominates global mean sea-level rise since 1970. *Nature Climate Change*, doi:10.1038/nclimate2991.
13. Dangendorf S (2016) Human influence on sea-level rise. *Nature Climate Change*, doi:10103-8/nclimate2994.
14. Hamlington BD, Thompson PR (2015) Considerations for estimating the 20th century trend in global mean sea level. *Geophys. Res. Lett*., 42, 4102-4109.
15. Thompson PR, *et al.* (2016) Are long tide gauge records in the wrong place to measure global mean sea level rise? *Geophys. Res. Lett.*, 43, 403-410.
16. Wöppelmann G, Marcos M (2016) Vertical land motion as a key to understanding sea level change and variability. *Rev. Geophys*., 54, 64-92, doi:10.1002/2015RG000502.
17. Peltier WR (2004) Global glacial isostacy and the surface of the Ice-Age Earth: The ICE5G(VM2) model and GRACE. *Ann. Rev. Earth. Planet. Sci*., 32, 111-149.
18. Marzeion B, Jarosch AH, Hofer M (2012) Past and future sea-level change from the surface mass balance of glaciers. *The Cryosphere*, 6, 1295-1322.
19. Kjeldsen KK, *et al.* (2015) Spatial and temporal distribution of mass loss from the Greenland ice sheet since AD 1900, *Nature*, 528, 396-400.
20. Frederikse T., *et al.* (2016), Closing the sea level budget on a regional scale: Trends and variability on the Northwestern European continental shelf, *Geophys. Res. Lett.*, 43, 864-872.
21. Veit E, Conrad CP (2016) The impact of groundwater depletion on spatial variations in sea level change during the past century, *Geophys. Res. Lett*., 43, 3351-3359.
22. Fiedler JW, Conrad CP (2010) Spatial variability of sea level rise due to water impoundment behind dams, *Geophys. Res. Lett*., 37, L12603.
23. Thompson PR, Merrifield MA (2014) A unique asymmetry in the pattern of recent sea level change. *Geophys. Res. Lett*., 41, 7675–7683.
24. Dangendorf S, *et al.* (2015) Detecting anthropogenic footprints in sea level rise. *Nature Communications*, 6, 7849.
25. Ruggieri E (2013) A Bayesian approach to detecting change points in climatic records, *Int. J. Climatol.*, 33, 520-528.
26. Hamlington BD, *et al.* (2016) Assessing the impact of vertical land motion on twentieth century global mean sea level estimates, *J. Geophys. Res*., 121, 4980-4993.
27. Kopp RE, *et al*. (2016) Temperature-driven sea-level variability in the Common Era. *Proc. Natl. Acad. Sci. USA*, 113, 1434–1441.
28. Marcos M *et al.* (2016) Internal variability versus anthropogenic forcing on sea level and its components. *Surveys in Geophysics*, doi:10.1007/s10712-016-9373-3
29. Wöppelmann G, *et al.* (2014) Evidence for a differential sea level rise between hemispheres over the twentieth century, *Geophys. Res. Lett*., 41, 1639-1643.
30. Rahmstorf S, et al. (2015) Exceptional twentieth-century slowdown in Atlantic Ocean overturning circulation, Nature Climate Change, 5, 475-480.
31. Levermann A, et al. (2005) Dynamic sea level changes following changes in the thermohaline circulation, *Climate Dynamics*, 24, 347-354.
32. Jevrejeva S, Grinsted A, Moore JC, Holgate S (2006) Nonlinear trends and multiyear cycles in sea level records. *J. Geophys. Res*., 111, C09012.
33. Ponte RM (2006) Low-frequency sea level variability and the inverted barometer effect. *J. Climate*, 23:4, 619-629.
34. Compo GP, *et al.* (2011) The Twentieth Century Reanalysis Project. *Quarterly Journal of the Royal Meteorological Society*, 137, 1-28.
35. Vorosmarty CJ, et al. (1997) The storage and aging of continental runoff in large reservoir systems of the world. *Ambio*, 26, 210-219.
36. Chao BF, Wu Y, Li Y (2008) Impact of artificial reservoir water impoundment on global sea level. *Science*, 320, 212-214.
37. Wada, Y., M.-H. Lo, P. J. F. Yeh, J. T. Reager, J. S. Famiglietti, R.-J. Wu, and Y.-H. Tseng (2016), Fate of water pumped from underground and contributions to sea-level rise, *Nature Clim. Change*, *6*, 777-780.
38. Wada Y, *et al.* (2012) Past and future contribution of global groundwater depletion to sea-level rise. *Geophys. Res. Lett*., 39, L09402.
39. Marzeion B, Leclercq PW, Cogley JG, Jarosch, AH (2015) Brief Communication: Global reconstruction of glacier mass change during the 20th century are consistent. *The Cryosphere*, 9, 2399-2404.
40. Noel B, *et al.* (2015) Evaluation of the updated regional climate model RACMO2.3: Summer snowfall impact on the Greenland ice sheet, *The Cryosphere*, 9, 1831-1844.
41. Mitrovica, J. X., J. Wahr, I. Matsuyama, and A. Paulson (2005), The rotational stability of an ice-age earth, *Geophys. J. Int.*, *161*, 491-506.
42. Tamisiea, M. E., E. M. Hill, R. M. Ponte, J. L. Davis, I. Velicogna, and N. T. Vinogradova (2010), Impact of selfattraction and loading on the annual cycle in sea level, *J. Geophys. Res.*, 115, C07004, doi:10.1029/2009JC005687.
43. Griffies SM, Greatbatch RJ (2012) Physical processes that impact the evolution of global mean sea level in ocean climate models. *Ocean Model.*, 51, 37–72.
44. Carton FM, Giese BS (2008) A reanalysis of ocean climate using Simple Ocean Data Assimilation (SODA). *Mon. Weather Rev*., 136, 2999–3017.
45. Bamber J, Riva REM (2010) The sea level fingerprint of recent ice mass fluxes. The Cryosphere, 4, 621-627.
46. Visser H, Dangendorf S, Peterson A (2015) A review of trend models applied to sea level data with reference to the "acceleration-deceleration debate". *J. Geophys. Res*., 120, 3873-3895.
47. Bos MS, Williams SDP, Araujo IB, Bastos L (2014) The effect of temporal correlated noise on the sea level rate and acceleration uncertainty. *Geophys. J. Int.*, 196, 1423-1430.
48. Dangendorf S, *et al.* (2014) Evidence for long-term memory in sea-level. *Geophys. Res. Lett.*, 41, 5564-5571.
49. Becker M, Karpytchev M, Lennartz-Sassinek S (2014) Long-term trends in sea level: natural or anthropogenic? *Geophys. Res. Lett*., 41, 5571-5580.
50. Ocana V, Zorita E, Heimbach P (2016) Stochastic secular trends in sea level rise. *J. Geophys. Res*., 121, 2183-2202.

Acknowledgements: We thank Aimee Slangen for providing her GMSL estimates based on historical CMIP5 runs. Ben Marzeion is acknowledged for sharing his updated glacier model including novel estimates for Antarctic glaciers. We are further grateful to Phil Thompson for providing the geographical regions of his cluster analysis, which was the basis for the selection of our regions. SONEL is acknowledged for providing comprehensive access to GPS data, which are available thanks to the institutions which contribute their observations freely. Alvaro Santamaria Gomez and Médéric Gravelle are acknowledged for calculating the GPS derived VLM estimates and their corresponding uncertainties. S.D. acknowledges a visiting fellowship of the University of the Balearic Islands, the BMBF-project AMSeL-Ostsee (03KIS0114), and the internally funded project PEPSEA at the University Siegen. M.M. acknowledges a "Ramon y Cajal" contract and the research project CLIMPACT (CGL2014-54246-C2-1-R) both funded by the Spanish Ministry of Economy. C.P.C. acknowledges funding from NSF grant EAR-1151241 and Research Council of Norway Centre of Excellence project 223272. R.E.M.R. and T.F. are grateful to the financial support by VIDI grant 864.12.012 from the Netherlands Organisation for Scientific Research (NOW).

Author contributions: S.D. and M.M. designed and performed the research and wrote the first draft of the paper; G.W., C.P.C. , R.E.M.R. and T.F. calculated the VLM and geoid corrections; all authors shared ideas and contributed to the writing.

Author contributions: S.D. and M.M. designed and performed the research and wrote the first draft of the paper; G.W., C.P.C. , R.E.M.R. and T.F. calculated the VLM and geoid corrections; all authors shared ideas and contributed to the writing.